

Article

Not peer-reviewed version

---

# In vitro Antimicrobial Efficacy of a New TiO<sub>2</sub>-Cu Coated Titanium Surface for Biomedical Applications

---

[Mahalakshmi Pandian](#)<sup>+</sup>, [Sacha Cavalier](#)<sup>\*,†</sup>, [Simone Guttai](#), [Philipp Kobbe](#), [Silvia Cometta](#), [Dietmar W Hutmacher](#)

Posted Date: 24 August 2025

doi: 10.20944/preprints202508.1680.v1

Keywords: surgical site infection; copper; intramedullary nail; titanium implants; *S. aureus*; antibacterial surfaces; metallic coatings



Preprints.org is a free multidisciplinary platform providing preprint service that is dedicated to making early versions of research outputs permanently available and citable. Preprints posted at Preprints.org appear in Web of Science, Crossref, Google Scholar, Scilit, Europe PMC.

Copyright: This open access article is published under a Creative Commons CC BY 4.0 license, which permit the free download, distribution, and reuse, provided that the author and preprint are cited in any reuse.

Disclaimer/Publisher's Note: The statements, opinions, and data contained in all publications are solely those of the individual author(s) and contributor(s) and not of MDPI and/or the editor(s). MDPI and/or the editor(s) disclaim responsibility for any injury to people or property resulting from any ideas, methods, instructions, or products referred to in the content.

Article

# In vitro Antimicrobial Efficacy of a New TiO<sub>2</sub>-Cu Coated Titanium Surface for Biomedical Applications

Pandian M. <sup>1,2,†</sup>, Cavalier S. <sup>1,2,3,\*†</sup>, Guttan S. <sup>4,5</sup>, Cometta S. <sup>2,3,7,8</sup>, Kobbe P. <sup>5,6</sup>,  
Hutmacher D. W. <sup>1,2,3,7,8</sup>

- <sup>1</sup> Australian Research Council Training Centre for Cell and Tissue Engineering Technologies, Queensland University of Technology, Australia.
  - <sup>2</sup> School of Mechanical, Medical and Process Engineering, Faculty of Engineering, Queensland University of Technology, Australia.
  - <sup>3</sup> Max Planck Queensland Centre for the Materials Science of Extracellular Matrices, Queensland University of Technology, Australia
  - <sup>4</sup> Stryker Trauma GmbH, Schönkirchen, Germany.
  - <sup>5</sup> Department for Trauma and Reconstructive Surgery, University Hospital of the Martin Luther University Halle, Halle (Saale), Germany.
  - <sup>6</sup> Department for Trauma and Reconstructive Surgery, BG Klinikum Bergmannstrost Halle, Halle (Saale), Germany.
  - <sup>7</sup> Australian Research Council Training Centre for Multiscale 3D Imaging, Modelling, and Manufacturing, Queensland University of Technology, Australia.
  - <sup>8</sup> Centre for Biomedical Technologies, Queensland University of Technology, Australia.
- \* Correspondence: [sacha.cavelier@qut.edu.au](mailto:sacha.cavelier@qut.edu.au)
- † These authors contributed equally

## Abstract

Despite advancements in surgical care, the management of surgical site infections (SSIs) associated with fracture-fixation devices is still a challenge after implant fixation, especially in open fractures. *Staphylococcus aureus* (*S. aureus*) is a common pathogen of SSIs and contaminates by penetrating the trauma itself (preoperatively) or during insertion of the fixation device (intraoperatively). A unique technology was developed to address this issue, consisting of an antibacterial surface obtained after depositing copper on a porous titanium oxide surface. This study aims to characterize and evaluate the *in vitro* bactericidal effect of this surface against *S. aureus*. Furthermore, the topography, elemental composition and other physicochemical properties of the copper coating were determined. *In vitro* assays have demonstrated a reduction of up to 5 log<sub>10</sub> in the bacteria colonization and additional quantitative and qualitative methods further supported these observations. This study illustrates the antibacterial efficacy and killing mechanisms of the surface, therefore proving its potential for minimising infection progression post-implantation in clinical scenarios and bringing important insights for the design of future *in vivo* evaluations.

**Keywords:** surgical site infection; copper; intramedullary nail; titanium implants; *S. aureus*; antibacterial surfaces; metallic coatings

## 1. Introduction

Surgical site infections (SSIs) are one of the most challenging complications associated with fracture and orthopaedic implants, especially in the case of open fractures, for which the infection rate can range from 10% to 50% [1,2]. In the case of open tibia fractures, the incidence rate of SSIs

varies from 5 to 30% [3–6]. SSIs can lead to delayed fracture healing, functional loss, amputation and patient morbidity, and the hospitalisation length increases to more than 7–11 days [7,8]. Additionally, fracture-related SSIs are associated with increased healthcare costs since treatments are up to 6.5 times more expensive for infected patients [9,10]. In the US, the financial burden of infected revisions was estimated to be \$1.62 billion in 2020 [11]. SSIs are therefore the most dominant driver for the total healthcare costs related to the surgical treatment of tibial fractures [12,13].

Most SSIs are reported to be associated with *Staphylococcus aureus* (*S. aureus*). The prevalence of these bacteria in SSIs has increased from 16.6% to 30.9% between 1992 and 2002 [14], reaching 37% in community hospitals [15]. Peri-implant *S. aureus* infections are challenging to treat, and conventional treatments require revision surgeries and long-term systemic antibiotic treatments. Current approaches consist of surgically removing the infected tissue and administering antibiotics, typically for 6–12 weeks [16–18]. Unlike other infections, implant-associated infections usually do not heal spontaneously, and prolonged antibiotic therapy can lead to the development of antibiotic resistance [19]. Antibiotic resistance is a growing concern as *S. aureus* tends to evolve into methicillin-resistant *S. aureus*, for which the number of isolates has risen from 9.2% to 49.3% [14]. In addition, the invasiveness and functional complications of surgical revisions have contributed to see antimicrobial surfaces as an alternative therapy to circumvent the limitations associated with systematic antibiotic treatments [20,21].

Antimicrobial surfaces for titanium (Ti) implants are used to fulfill two requirements: (1) prevent infection and (2) enhance fracture repair [22]. Antibiotic-coated nails for orthopaedic trauma surgery have been widely investigated [23–26] and enable the local release of drugs, resulting in bacterial reduction and improvements in bone healing [27]. However, they do not address concerns related to antibiotic resistance. Antiseptic coatings are presented as an alternative due to their broad-spectrum antibacterial, antiviral, and antifungal properties [28–30]. For instance, fluoride-doped TiO<sub>2</sub> coating on Ti implants [31], titanate-iodine coating [32] or iodine-coated Ti implants [33] exhibited superior antimicrobial activity against various bacteria and fungi. However, antiseptic coatings can interfere with the integration of the implant into surrounding tissue, cause allergic reactions [34], and their effectiveness diminishes over time, adding complexity and cost [35]. Nanostructured surfaces have also emerged as a key method for eradicating bacteria by controlling adhesion or friction, or even by inducing structural damage and oxidative stress. These surfaces include a wide variety of textures, such as nanoripples, nanopillars, nanotubes, nanowires, nanoprotusions or nanoparticles [36–38]. Nanostructured surfaces also include superhydrophobic surfaces, which deter bacterial colonization due to their water-repellent nature [39]. However, their lack of durability and resistance to corrosion limits their efficacy [40], and they fail to combine both efficiency and economic feasibility, as the fabrication techniques are too expensive at a large scale [36].

Finally, seventeen metal elements are known today to have antimicrobial activity [41,42], with silver (Ag), zinc (Zn), or copper (Cu) being the most used [43]. They possess a broad spectrum of antibacterial properties that assist in the prevention of bacterial implant contamination, particularly in surgical equipment [44]. Bactericidal mechanisms primarily consist of contact-killing, where bacteria are killed upon contact with the metallic elements at the surface [45,46]. For instance, Ag-coated Ti implants can significantly reduce bacterial contamination by disrupting the cell wall and affecting cellular metabolism [45]. Zn and its oxide, ZnO, exhibit antimicrobial properties against a wide array of microorganisms, including drug-resistant bacteria [47], and antiviral properties, as it disrupts viral protease and RNA or DNA polymerase functions, alongside viral attachment [48]. However, Ag and Zn can be cytotoxic, inhibiting both cell growth and tissue healing around the implant site [49,50]. In some cases, bacterial strains can develop resistance to Ag over time, reducing its effectiveness in preventing infection [49].

Cu, the most widely used bactericidal metallic coating, is a trace element in the human body, and therefore exhibits a high cytocompatibility and lower levels of toxicity, alleviating the limitations previously mentioned [51,52]. Unlike other metals, Cu has a lower likelihood of developing resistance to bacteria [51,53]. It is already employed in a variety of products, including door handles, handrails,

and textiles, as well as in biomedical applications and healthcare settings, such as intrauterine devices, bed linens, patient gowns, and wound dressings [54]. Indeed, Cu exhibits proficient contact-killing and inhibits bacterial growth [51]. The release of Cu ions, specifically  $\text{Cu}^+$  and  $\text{Cu}^{2+}$ , may cause damage to the bacterial membrane, thereby decreasing cell invasion and triggering an oxidative stress response that leads to lipid peroxidation, membrane disruption, protein impairment, and cell death [41,52,53]. As a result, essential cellular components leak out, contributing to bacterial death [52]. Additionally, Cu ions can penetrate the bacteria, causing DNA damage and disrupting vital cellular processes such as replication and transcription [55]. Overall, the multifaceted antibacterial mechanisms of Cu target various cellular components and processes, making it an effective antimicrobial agent [52]. Cu alloys have proven effectiveness against a wide spectrum of pathogens, rapidly eradicating 107 *S. aureus* cells per ml within 10 minutes, *Acinetobacter* within 240 minutes, or *E. coli* within 350 minutes, therefore reducing the bacterial inoculum by a factor of 105 [43]. Other studies on Cu coatings and Cu alloys have demonstrated significant *in vitro* reductions of *S. aureus*, by factors ranging from 103 to 1010 after a few hours [53,56–58], with greater efficacy observed in moist environments [56].

A novel electrochemical coating process was developed to deposit metallic Cu at the surface of medical-grade Ti implants. Such a technology could have direct biomedical applications, such as intramedullary nails with bactericidal coatings for bone fracture repairs. However, the evaluation of the physico-chemical and antimicrobial properties has only just been initiated in recent work from Giraldo-Osorno et al. [59]. We propose an extended characterization of the surface using additional techniques, along with a reproduction of the *in vitro* antibacterial evaluation against *S. aureus*, but with extra time points and higher concentrations. These additional data will be central for the design of future *in vivo* evaluations. The hypothesis that the novel Cu coating on Ti is capable of rapidly decreasing bacterial colonization on the implant surface over time *in vitro* after inoculation of the strain, when compared to bare Ti, will be tested. If successful, the outcomes will pave the way for future *in vivo* evaluations in large animal infection models and will accelerate the regulatory approval of Cu-coated orthopaedic implants.

## 2. Methods

### 2.1. Materials

Discs made of Ti6Al4V alloy with a diameter of 12 mm and a height of 3 mm were manufactured by Stryker Trauma GmbH, Schönkirchen, Germany. Control Ti discs were anodized, cleaned, sterile packed, and gamma-sterilized at 25-50 kGy (control discs group, or C-D). Anodizing, as well as the antibacterial coating, were developed and carried out by DOT GmbH (DOT GmbH, Rostock, Germany). A porous Ti oxide ( $\text{TiO}_2$ ) layer was deposited according to the principle of anodic spark discharge (Figure 1A), followed by the deposition of Cu into the pores by electrochemical methods (Figure 1B-C). The excess of Cu and  $\text{TiO}_2$  was removed through the glass bead blasting technique (Figure 1D-E). The Cu-coated discs (Cu-D group) were then cleaned and sterile packed using gamma-sterilization (25-50 kGy) for further experimentation. Final discs are displayed in Figure 1 F, illustrating that a slight darker colour was observed on the Cu-D discs compared to the C-D discs.

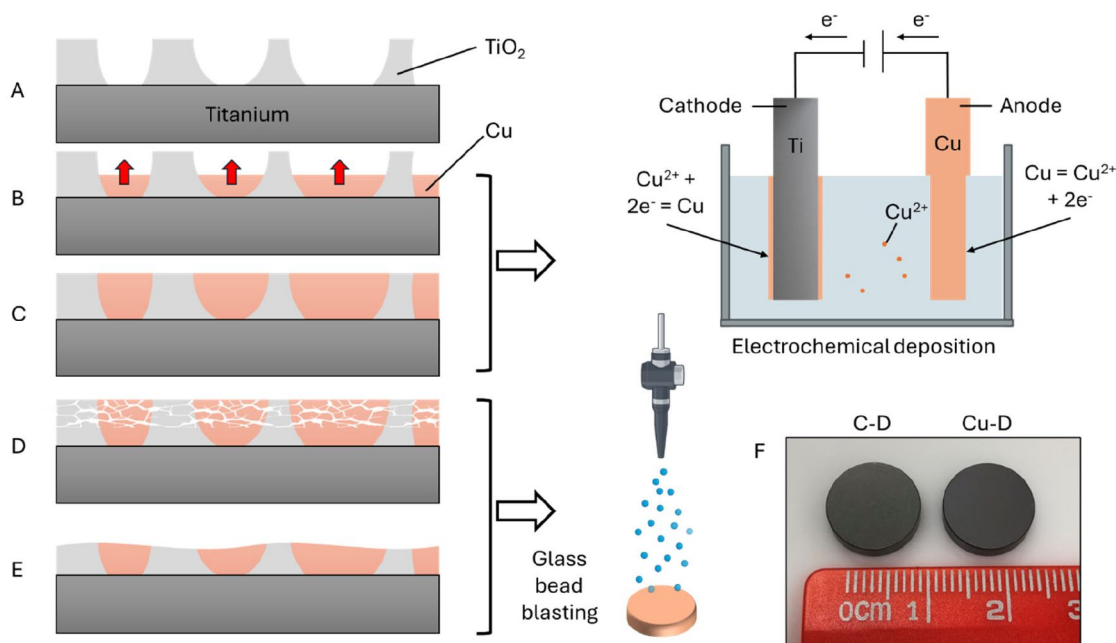


**Figure 1.** Schematic diagram of the fabrication process: A) A porous TiO<sub>2</sub> layer was formed. B-C) Cu was deposited into the pores by electrochemical deposition. D-E) Glass bead blasting was used to remove the excess Cu and friable TiO<sub>2</sub>. F) View of the C-D and Cu-D discs.

Finally, *S. aureus* subsp. *aureus* Rosenbach ATCC 6538 (ATCC® 6538-MINI-PACK™, ATCC, Manassas, Virginia, USA) was used in this study.

### 2.1. Scanning Electron Microscopy (SEM) and Energy Dispersive Spectroscopy (SEM-EDS)

The microstructure of the three C-D and three Cu-D samples was analysed using SEM (MIRA3 FEG-SEM, TESCAN, Brno, Czech Republic). The samples did not receive additional metallic coating since they are conductive materials. Plasma cleaning (Evactron® 25Z & Soft Clean, Zephyr, Sydney, Australia) was performed for 5 minutes before imaging to remove impurities. High-resolution images were captured at 5 kV voltage and 8 W/m<sup>2</sup> beam intensity in backscattered detector mode, at a working distance of 8 mm. Image analysis was conducted with the software ImageJ (<https://imagej.net/ij/>), employing binary image analysis and colour histogram. The chemical composition of the samples was investigated by EDS (Phenom XL G2 Desktop SEM, ThermoFisher Scientific, Australia) immediately after imaging with the SEM. For this purpose, the SEM was operated at a magnification of 1000X, with a voltage of 15 kV and a working distance of 10 mm, and one sample per group was analysed in six different locations.

The bacterial morphology of *S. aureus* on two Cu-D and two C-D samples at different incubation times (4h, 24h, 72h, details in section 2.9) was also observed using the SEM instrument, with the same settings. For this purpose, after fixing the bacteria in 4% (v/v) paraformaldehyde (PFA) solution, the samples were dehydrated using ethanol baths with progressively increasing concentrations (10 min in 20 to 100% ethanol, increment of 10% each time). The samples were critical point dried and sputter-coated with a 2 nm platinum conductive layer.

### 2.2. Inductively Coupled Plasma Optical Emission Spectroscopy (ICP-OES)

C-D and Cu-D samples were transferred and accurately weighed into 50 ml polypropylene digestion tubes before the addition of 5 ml of a 1:1 HNO<sub>3</sub>:H<sub>2</sub>O mixture prepared from twice sub-boiling distilled HNO<sub>3</sub> and deionized water. The samples and solutions were then briefly agitated on an ultrasonic bath for 60 seconds before being placed on a graphite heating block set at 110°C for 45 minutes twice. Residual liquids were transferred into aliquots for analysis by ICP-OES using a

combination of axial and radial viewing modes. This was achieved using an Optima 8300 ICP-OES (Perkin Elmer, Waltham, Massachusetts, USA) fitted with an ESI SC-4DX autosampler and PrepFAST 2 sample handling unit for online internal standardisation, auto-dilution of samples and calibration standards.

### 2.3. X-ray Photoelectron Spectroscopy (XPS)

The elemental composition of the surface of three C-D and three Cu-D samples was analysed using XPS (AXIS Ultra, Kratos Analytical, Manchester, UK). Initial survey spectra were obtained at a pass energy of 160 eV to provide an overview of the surface elements. Subsequently, high-resolution scans of specific elements (O 1s, C 1s, Ti 2p, Cu 2p, Al 2p, and Si 2p) were conducted at a pass energy of 20 eV, allowing for a more detailed analysis of their chemical states and concentrations. Atomic concentrations of the elements present on the surface were calculated from the survey spectra using the CasaXPS software.

### 2.4. Profilometry

The surface roughness and micro-topography were examined by a profilometer (Dektak XTL, Bruker, Billerica, Massachusetts, USA) which measures roughness parameters according to ISO 4287/2000 standards.  $R_a$  (roughness calculated by arithmetical mean deviation) was calculated upon acquisition of data for three C-D and three Cu-D samples following the formula:

$$R_a = \frac{1}{n} \sum_{i=0}^n |\gamma_i| \quad (1)$$

where  $n$  denotes the number of data points within the sampling length and  $\gamma_i$  represents the difference between the actual height at a specific data point and the mean height of the sampling length.

### 2.5. Sessile Dynamic Contact Angle

The surface wettability was assessed using the sessile drop technique with a contact angle meter (ThetaFlex Drop Shape Analyser, Biolin, Gothenburg, Sweden). The contact angle of the surface of three C-D and three Cu-D samples was determined using 5  $\mu$ l droplets of distilled water at room temperature. The image of the water droplet spreading and retraction was captured for 10 seconds after delivery. High-speed cameras and contact angle goniometers with video capturing capabilities were used to record the dynamic behaviour. The images were used to automatically measure the contact angle over time through the instrumental software.

### 2.6. Cu Release Profile

The assessment of the Cu release profile of the coating was adapted from a protocol by Giraldo-Osorno et al. [59] who determined the release kinetics up to 7 days. In the present study, the Cu release experiment was extended to 14 days. The Cu leaching behaviour of three Cu-D samples was assessed in 1 ml of Dulbecco's modified Eagle medium with fetal bovine serum at 37°C to mimic the body fluid. The Cu<sup>2+</sup> release was measured using ICP-OES (Optima 8300, Perkin-Elmer, Waltham, Massachusetts, USA) according to the ISO 10993-12 standard. At each time point, the media was replaced and transferred into polypropylene digestion tubes along with a 1:1 HNO<sub>3</sub>:H<sub>2</sub>O mixture. After ultrasonic agitation and heating at 110°C for 45 mins, followed by a subsequent 60-minute heating with additional water, the samples were cooled, decanted, and transferred for analysis to measure the cumulative Cu<sup>2+</sup> concentration to evaluate their release behaviour.

### 2.7. Optical Densitometry

In this study, the target bacterial concentration of 1–5 × 10<sup>8</sup> CFU/ml corresponded to an optical density (OD<sub>600</sub>) of 0.06. *S. aureus* was grown overnight on Mueller-Hinton agar plates, then

resuspended in Tryptone Soya Broth (TSB) and measured at 600 nm using a Beckman DU 800 Spectrophotometer (Beckman Coulter, Brea, USA). The actual bacterial concentration in the broth was determined by serial dilution, as detailed in the next paragraph.

### 2.8. Antibacterial Activity Assay Measured by CFU Count

All CFU count analyses in this study were performed by the serial dilution technique. Serial dilutions of each sample were plated on Mueller Hinton agar and incubated overnight. The count of individual colonies was facilitated by imaging via ChemiDoc Imaging System (Bio-Rad, Hercules, CA, USA).

For the antibacterial activity assay, a protocol was adapted from similar studies on different surfaces [60–63], and from Giraldo-Osorno et al. [59], who evaluated the same Cu coating. Here, the *in vitro* evaluation was extended by using an additional time point (72 hours) and a higher bacterial inoculum. *S. aureus* bacteria were defrosted and streaked onto agar plates to produce fresh cultures upon overnight incubation. To prepare a 0.5 McFarland standard suspension (corresponding to a turbidity of 0.06 OD<sub>600</sub> value at 600 nm, equivalent to  $1-5 \times 10^8$  CFU/ml), single *S. aureus* colonies from the streak plate were suspended in TSB. OD<sub>600</sub> measured the initial concentration at  $t = 0$ h, and a more accurate measurement of the number of CFU was performed later by the serial dilution technique. 1 ml of bacterial suspension was added to twenty-four C-D samples (positive control group) and twenty-four Cu-D samples (experimental group), which were incubated at intervals of 4h, 24h, and 72h. In addition, twenty-four C-D samples received sterile TSB (negative control group) and were incubated at the same intervals, to detect potential cross-contamination. At 4h and 24h, six discs of each group (negative control, positive control, and experimental) were washed twice with 500  $\mu$ l of sterile PBS and subsequently sonicated twice for 15 minutes in 2 ml of sterile PBS to recover the adhered bacteria. The CFU counting was achieved by serial dilution of the recovered bacterial cultures on Mueller-Hinton agar plates, upon overnight incubation. The remaining discs (twelve for each group) were incubated for 72h, but half of the discs had their media changed at 24h and 48h, to eliminate the accumulation of Cu released from the Cu-D samples in the media, as well as to provide fresh nutrients for bacterial growth. Table 1 summarises the different groups evaluated in this assay. After 72h, the samples underwent the same protocol as the other time points (washed twice in 500  $\mu$ l of sterile PBS, sonicated twice for 15 minutes in 2 ml of sterile PBS and serially diluted and plated on Mueller-Hinton agar).

**Table 1.** Groups and time points evaluated in the antibacterial assay.

Group		Time points & media change
Negative control	C-D sample	4h, 24h, 72h
	No bacteria	No media change
		72h
Positive control	C-D sample	4h, 24h, 72h
	<i>S. aureus</i> ,	No media change
	$1-5 \times 10^8$ CFU/ml	72h
		Media change at 24h and 48h
Experimental	Cu-D sample	4h, 24h, 72h
	<i>S. aureus</i> ,	No media change
	$1-5 \times 10^8$ CFU/ml	72h
		Media change at 24h and 48h

### 2.9. Presto Blue

Six samples each of C-D and Cu-D were placed into the wells of a 24-well plate. Each sample was then inoculated with 1 ml of *S. aureus* suspension ( $1-5 \times 10^8$  CFU/ml) in Luria-Bertani (LB) broth and incubated at 37°C for different time intervals (4h, 24h, 72h). After each time point, the respective

C-D and Cu-D samples underwent a double PBS wash, followed by transfer to a new well plate. A 1X solution of Presto Blue reagent was diluted in LB broth (1:10 dilution) and 500  $\mu$ l were added to each C-D and Cu-D containing well and incubated at 37°C for 1h. Afterward, elutes were transferred to a 96-well plate in triplicate, and fluorescence was quantified using a plate reader (excitation: 560 nm, emission: 590 nm). The remaining Presto Blue and LB broth solutions were discarded, and the disc-containing wells were washed twice with LB broth before being refilled with fresh LB broth. The plate was re-incubated at 37°C until the next time point. The procedure was repeated for each time point.

### 2.10. Live - Dead Staining for Confocal Imaging

*S. aureus* stock solution was cultured in LB broth for 24 hours, and the concentration was adjusted to 0.5 McFarland, as previously described. The suspension containing approximately  $1-5 \times 10^8$  CFU/ml was added to Cu-D samples placed in a 48-well plate and incubated at 37°C for 4h, 24h or 72h. Post-incubation, the discs were washed, stained for 15 min with Syto 9 and propidium iodide (PI) dyes, and fixed with 4% (v/v) PFA. Live and dead bacteria were detected by fluorescent imaging with a confocal microscope (Leica TCS SP5, Leica Microsystems, Wetzlar, Germany). The sequence was repeated for each time point (4h, 24h and 72h).

### 2.11. Statistical Methods

All experimental data were expressed as average  $\pm$  standard deviation (SD). Statistical comparisons between groups were performed by calculating p-values using a two-tailed, homoscedastic student's t-test for pairwise comparisons. Statistical significance was defined as  $p < 0.05$ .

## 3. Results

### 3.1. SEM Observation and EDS Elemental Analysis

SEM and EDS elemental analysis were initially used to assess the morphology and elemental composition of the C-D and Cu-D surfaces. Areas with brighter contrast were observed on the samples from Cu-D group, as shown in Figure 2B, but not in the C-D group, as shown in Figure 2A. Those contrasted areas can be attributed to the presence of Cu, because of the difference in conductivity between Cu and Ti. Cu particles were randomly and densely arranged onto the Ti surface, exhibiting a range of sizes between 0.5 and 5  $\mu$ m. Upon analysis of the corresponding binary images using ImageJ, the Cu coverage of the surface was calculated to be  $31.0 \pm 5.0$  %. Similar observations were reported by Giraldo-Osorno et al. [59] who characterized the same coating technology and described the surface as *island-like Cu deposits*.

Figure 2C and 2D show the energy-versus-intensity spectra obtained by EDS analysis for the C-D and Cu-D samples, respectively. The intensity peaks of the C-D samples' spectra were characteristic of the presence of oxygen (O), aluminium (Al), silicon (Si), Ti, vanadium (V). The presence of Ti, Al, and V in the C-D samples, and the proportion of these elements, given by Supplemental Table S1, followed the expected composition of medical grade Ti-4Al-6V alloy [64,65]. A similar composition was revealed in the Cu-D samples, but with Cu at a concentration of 23.1 w% (Supplemental Table S1). The presence of oxygen in high quantities was attributed to the presence of oxide forms of Ti, TiO<sub>2</sub>, on the surface that were deposited during the fabrication process. The decrease in the elemental composition when comparing Cu-D to C-D (e.g. 47.0 w% vs. 31.2 w% for Ti, 35.7 w% vs. 27.4 w% for O, or 4.9 w% vs. 3.6 w% for Al) is the result of Cu covering the surface instead of Ti-4Al-6V alloy or TiO<sub>2</sub>. Finally, the presence of Si was due to the glass bead blasting procedure, during which ceramics, including SiO<sub>2</sub>, were projected at the surface. The glass bead blasting process on Ti surfaces can indeed lead to the contamination of the surfaces by elements related to the composition of the beads, such as O, Si, sodium (Na), magnesium (Mg), and calcium (Ca) [65,66].

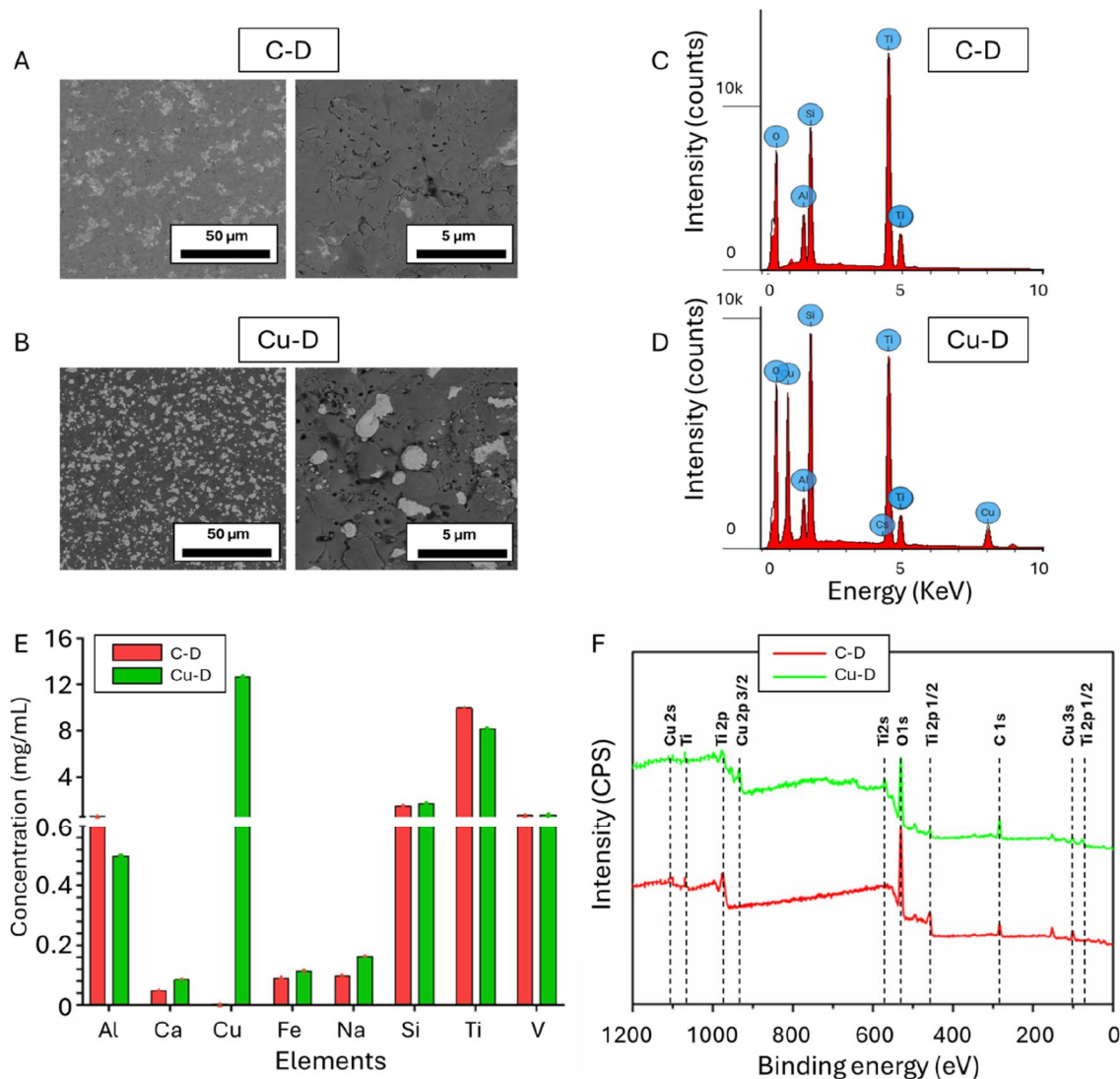
### 3.2. Cu Surface Elemental Concentration Measured Through Inductively Coupled Plasma Optical Emission Spectrometry (ICP-OES)

Figure 2E displays the results of the ICP-OES analysis, which was also used to quantify the elemental composition of C-D and Cu-D surfaces. The detected elements were similar to those detected with EDS, indicating the presence of Ti, Al, V, Si, and Cu in the Cu-D samples only. Additionally, as depicted in Supplemental Table S1, the higher sensitivity of the technique enabled the detection of additional elements such as Ca and Na, at low concentrations. This can be attributed to the glass bead blasting processing, which involves SiO<sub>2</sub>, Na<sub>2</sub>O, CaO, MgO, and Al<sub>2</sub>O<sub>3</sub> [65,66]. Iron (Fe) was also detected in low concentrations, as part of the composition of Ti-6Al-4V alloy [67]. Due to the different nature of the analysis, which consists in the dissolution of a thin layer at the surface of the samples, the proportion of the elements differed from the EDS analysis. For instance, the concentration of Cu detected with ICP-OES was lower, as a thicker layer of the TiO<sub>2</sub>-Cu coating may have been dissolved during the analysis.

### 3.3. X-Ray Photoelectron Spectroscopy (XPS)

Finally, the elemental composition of C-D and Cu-D samples was also investigated through XPS, and the survey spectra are shown in Figure 2F. Carbon, O, Ti, Si, and Na were detected in both groups, and Cu, and Al in Cu-D only. The presence of carbon is the result of residual organic contamination that could have persisted despite plasma cleaning. High-resolution spectra taken in the Ti 2p regions on the C-D and Cu-D samples' surface (Figure S1 in supplemental data) evidenced a peak characteristic of Ti<sup>4+</sup> (TiO<sub>2</sub>) at 459 eV, dominating with a lower oxidation state fitted for Ti<sup>3+</sup> at 461 and 464 eV. The Ti 2p spectrum depicts the typical binding energies of Ti dioxide (TiO<sub>2</sub>) [68] thus demonstrating the presence of TiO<sub>2</sub>. The Ti<sup>3+</sup> suggests that this oxidation state exists throughout the oxide layer. Similarly, to C-D, Cu-D exhibited the Ti<sup>4+</sup> without any Ti<sup>3+</sup> peak, indicating a reduction in the oxidation state of Ti in the TiO<sub>2</sub> form. This reduction was attributed to the presence of Cu in its oxidised form, with the impact of Cu deposition being obvious in Cu-D [68]. In contrast, in the Cu high-resolution spectra, C-D samples did not show any peaks for Cu and Cu-D samples showed peaks at 935 and 955 eV, thus evidencing the presence of Cu<sup>2+</sup>, Cu<sup>+</sup> or Cu species (Figure S1 in supplemental data). Moreover, the peaks of the Cu 2p at 935 and 955 eV can be attributed to the formation of Cu<sup>2+</sup> on the surface [69].

The atomic concentrations were calculated and are indicated in Supplemental Table S2. The alterations in the elemental makeup of oxygen, Ti, and Cu suggest that Cu has been successfully bonded to the surface of the Ti disc. The drop in Ti (1.5 versus 5.5%) and O (32.9 versus 50.5%) when comparing Cu-D to C-D indicates a reduction in elemental composition due to Cu covering the surface instead of Ti and its oxide form, TiO<sub>2</sub>. The presence of Al was primarily due to the composition of the bulk material (Ti6Al4V), while Si and Na were likely due to the glass beads sandblasting technique used during sample preparation.



**Figure 2.** SEM imaging of A) C-D sample and B) Cu-D sample, at two different magnifications. Intensity spectra of C) C-D sample and D) Cu-D sample. E) ICP-OES concentration analysis. F) Survey spectrum of the XPS analysis for the two groups.

### 3.4. Surface Profilometer

The surface profilometry results of the C-D and Cu-D groups are shown in Figure 3A. The average surface roughness  $R_a$  of C-D and Cu-D samples was  $418.7 \pm 41.7$  nm and  $479.0 \pm 64.5$  nm, respectively. This increase of roughness for the Cu-coated surface was also observed in the study by Giraldo-Osorno et al. [59]. Such a difference in roughness can be attributed to the presence of Cu at the surface of Cu-D samples. Indeed, the antibacterial coating consists of a combination of a hard and stiff porous  $\text{TiO}_2$  ceramic layer and more ductile Cu agglomerates. Because of the dissimilar mechanical properties of the two materials, it can be hypothesised that Cu and  $\text{TiO}_2$  were not removed in the same proportions during the blasting process, thus revealing a more irregular topography on the Cu-D sample surface. For instance, the Vickers hardnesses of Ti and  $\text{TiO}_2$  are 352 Hv [70] and 228 Hv [71] respectively, while Cu has a hardness of 107 Hv [72].

### 3.5. Contact Angle – Dynamic mode.

The contact angle measurements were evaluated through the sessile drop technique to reveal the wetting characteristics of the two different sample groups C-D and Cu-D (Figure 3B-C). For C-D

samples, the contact angle was  $73.5 \pm 6.0^\circ$  (versus  $70.23^\circ$  for Giraldo-Osorno et al. [59]) which indicates hydrophilicity. For Cu-D samples, however, a contact angle of  $98.0 \pm 2.5^\circ$  (versus  $105.05^\circ$  for Giraldo-Osorno et al.) was measured, indicating hydrophobicity. Similarly to roughness, this increase in the contact angle can be attributed to the glass blasting process, during which heterogeneous surfaces and micropores are created. Such micropores act as air cavities, which prevent spontaneous wetting [73]. These changes in the surface properties of the Cu-D group might affect bacterial adhesion. However, it is unclear whether this hydrophobicity contributes to the antibacterial efficacy by reducing bacterial adhesion on the surface, or if it alters the antibacterial activity by preventing bacteria adhesion before they are killed by the ions from the coating.

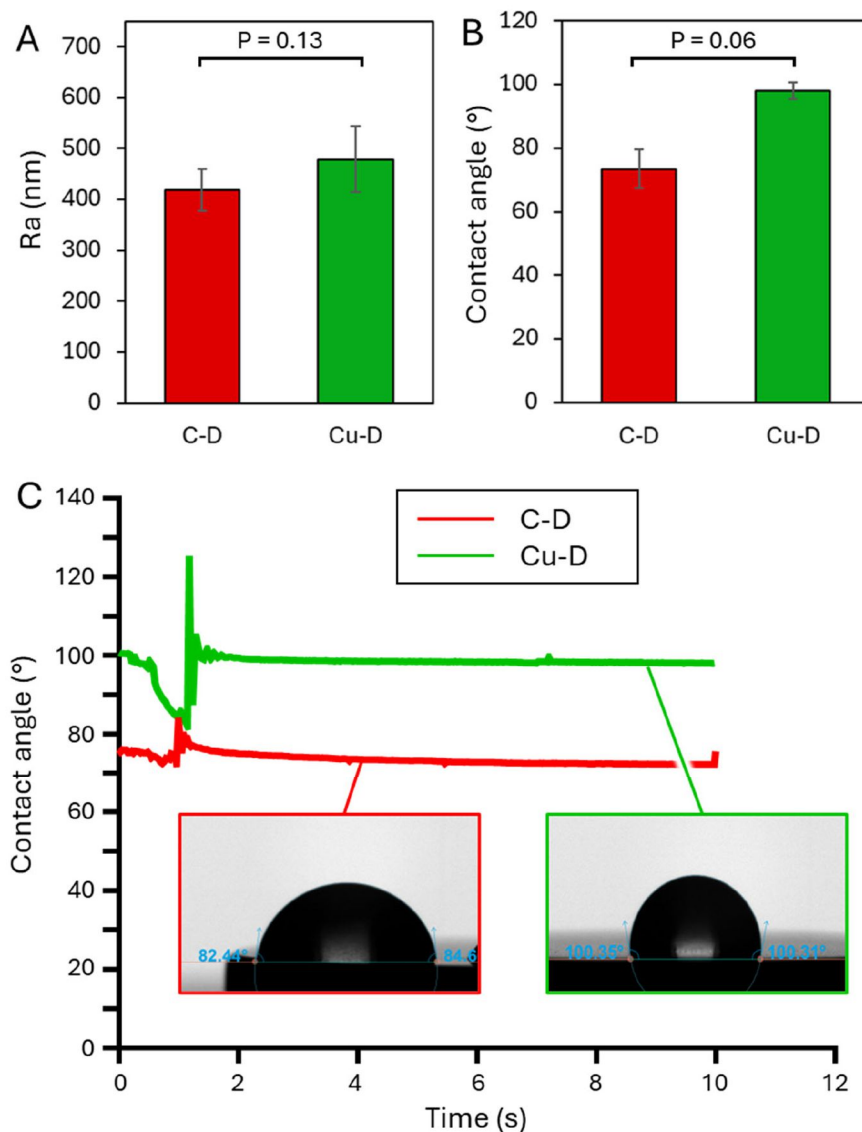


**Figure 3.** A) Surface roughness and B) contact angle measurements for the C-D and Cu-D groups. C) Evolution of contact angle over 12 seconds.

### 3.6. Cu Release Kinetics via ICP-OES

The cumulative release and release profile for Cu-D samples are shown in Figure 4. The release profile can be separated into two stages: an immediate burst release until day 3, and a low-rate release persisting until day 12. After day 13, no trace of  $\text{Cu}^{2+}$  was detected in the leachate, indicating that the

Ti surface had been cleared of Cu. During the burst release,  $224 \pm 43 \mu\text{g}$  were released after 24 hours, and  $326 \pm 87 \mu\text{g}$  after 72 hours, which correspond to 53% and 76% of the cumulative release after 14 days ( $425 \pm 113 \mu\text{g}$ ). The surface was therefore capable of releasing  $0.96 \mu\text{g}/\text{mm}^2$  within the first 3 days after release. Similar release kinetics for this coating, including the initial burst release in the 8 to 48h timeframe, were reported by Giraldo-Osorno et al.[59]. Here, we extended the release study up to 14 days and demonstrated that Cu release was still detectable up to 14 days, albeit in small quantities. These measurements of the  $\text{Cu}^{2+}$  release indicate that the quantities of Cu left on the surface after 72 hours may be low, thereby reducing the efficiency of the coating.

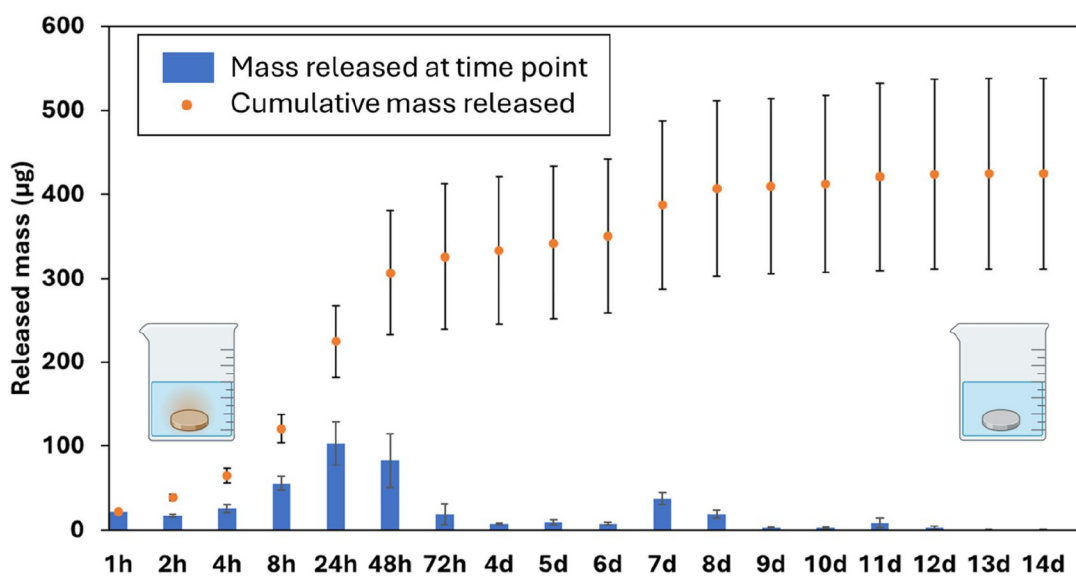


Figure 4. Cu release kinetics for a single Cu-D sample.

### 3.7. CFU Counting by Serial Dilution Technique

The CFU counting by serial dilution technique was used to evaluate the antibacterial activity of C-D and Cu-D samples and the results of the analysis are shown in Figure 5A. The bacterial concentration at  $t = 0\text{h}$  was initially estimated by  $\text{OD}_{600}$  measurement and subsequently confirmed by CFU counting, resulting in a final concentration of  $7.3 \times 10^8$  CFU/ml. In the negative control group (C-D samples, sterile PBS), CFU counts did not reveal any bacteria at the surface of the disc at any timepoints, confirming no cross-contamination. In contrast, CFU counts in the C-D group was  $4.2 \times 10^8$  CFU/ml at  $t = 4\text{h}$ ,  $1.7 \times 10^9$  CFU/ml at  $t = 24\text{h}$  and  $1.9 \times 10^7$  CFU/ml at  $t = 72\text{h}$ , indicating increasing bacterial colonization on the surface of the discs during the first 24 hours, followed by a slight decline at 72 hours. When the media was changed, the retrieved bacterial concentration was  $2.4 \times 10^7$  CFU/ml at  $t = 72\text{h}$ , showing that the change of media did not affect the population of bacteria adhering to the discs. In the Cu-D, group, the CFU counts of retrieved bacteria revealed consistent decline of the bacterial population, with  $4.6 \times 10^6$  CFU/ml at  $t = 4\text{h}$ ,  $2.7 \times 10^4$  CFU/ml at  $t = 24\text{h}$  and  $4.6 \times 10^3$  CFU/ml at  $t = 72\text{h}$ . When compared to C-D group, Cu-D discs underwent a  $2 \log_{10}$  bacterial colonization reduction after 4 hours ( $p < 0.05$ ), a  $4.8 \log_{10}$  reduction after 24 hours ( $p < 0.01$ ), and a  $3.6 \log_{10}$  reduction after 72 hours ( $p < 0.001$ ). These reductions indicate a significant bactericidal effect *in vitro*, as early as 4 hours, and extended to up to 24 hours. These results are comparable to the outcomes from other studies on Cu coatings and Cu alloys against the same bacteria *in vitro*, where 3 to  $10 \log_{10}$  reduction were observed [53,57,58]. For instance, the study from Giraldo-Osorno et al. [59] used an initial concentration of  $10^5$  CFU/ml. It revealed a higher reduction of the bacterial population after 4 hours, with 3.16 and 3.96  $\log_{10}$  reduction when cultured in TSB and Roswell Park Memorial Institute 1640 (RPMI) media, and respectively 1.2 and 8.02  $\log_{10}$  reductions at 24 hours. In addition, when the bacteria media was changed every 24 hours, the antibacterial effect was much less pronounced, since bacterial population adhered to the Cu-D samples was  $5.1 \times 10^6$  CFU/ml, which was only 5 times less

than the bacterial population in the C-D group. This can be attributed to a diminished contact killing mechanism, as the Cu is mostly released at 72 hours, along with the absence of accumulated Cu in the freshly renewed medium that could have controlled the bacterial growth. Indeed, each disc released approximately 224  $\mu\text{g}$  of Cu within the first 24h according to the Cu release kinetics experiments (Figure 4), and the concentration of Cu could have exceeded the minimal bactericidal concentration (MBC) against *S. aureus* (160  $\mu\text{g}/\text{ml}$  [74]). For instance, Giraldo-Osorno et al [59] pre-conditioned two culture media (TSB and RPMI) by immersing the Cu-coated discs for 24 hours before culturing the bacteria, and measured 0.78 and 9.3  $\log_{10}$  reductions after 24h. In addition, the bacterial concentration measured at 72h on the Cu-D samples with media changed every 24h was close to that measured at 4h (5.1 versus  $4.6 \times 10^6$  CFU/ml). The previous results on the Cu release kinetics showed that each disc released 65  $\mu\text{g}$  in the first 4h, and 19  $\mu\text{g}$  between 48h and 72h. It is therefore likely that the remaining Cu at the surface of the disc at 72h still contributed to the reduction of bacterial population via contact killing mechanism, which compensated for the diminished bactericidal effect of the lower concentration of Cu in the media.

Overall, these results indicate that the increased concentration of Cu in the medium had a bactericidal effect, in parallel to the known contact killing mechanism widely reported in literature for this type of metallic coating. Local Cu concentrations may also vary drastically around a Cu-coated device in a clinical scenario or in an *in vivo* context. In this *in vitro* assay, two extreme scenarios were tested, one with an accumulation of Cu in the media and only one bacterial challenge, and one with three bacterial challenges and a reduction of Cu ions in solutions due to the media change. The resulting observations presented here could assist the interpretations of future *in vivo* evaluations. Indeed, due to the combined effect of contact killing and the increasing Cu concentration around a Cu-coated device, the results obtained from animal models evaluating the efficacy of the coating may depend on the inoculation method. Bone infection models in large animals using collagen sponges to inoculate the bacteria [111–114], might not fully benefit from the contact killing mechanism. On the other hand, animal models that mimic a clinical scenario by inoculating the bacteria directly on or around the bactericidal implant can demonstrate the combined effect of contact killing and increasing Cu concentration around the device.

### 3.8. Presto Blue Assay

The metabolic activity of C-D and Cu-D was evaluated at  $t = 4\text{h}$ ,  $24\text{h}$ , and  $72\text{h}$  after incubation using the Presto Blue assay (Figure 5B). When compared to C-D samples, the fluorescence of Cu-D samples exhibited a 6-fold drop at 4 hours, a 5-fold decrease at 24 hours, and a 7-fold decrease at 72 hours, with a statistical significance level below 0.01 at all time points, indicating a significant reduction in bacterial metabolic activity for the Cu-D group when compared to the C-D group. The reduction of both the metabolic activity and bacterial concentration supports the antibacterial efficacy of the coating.

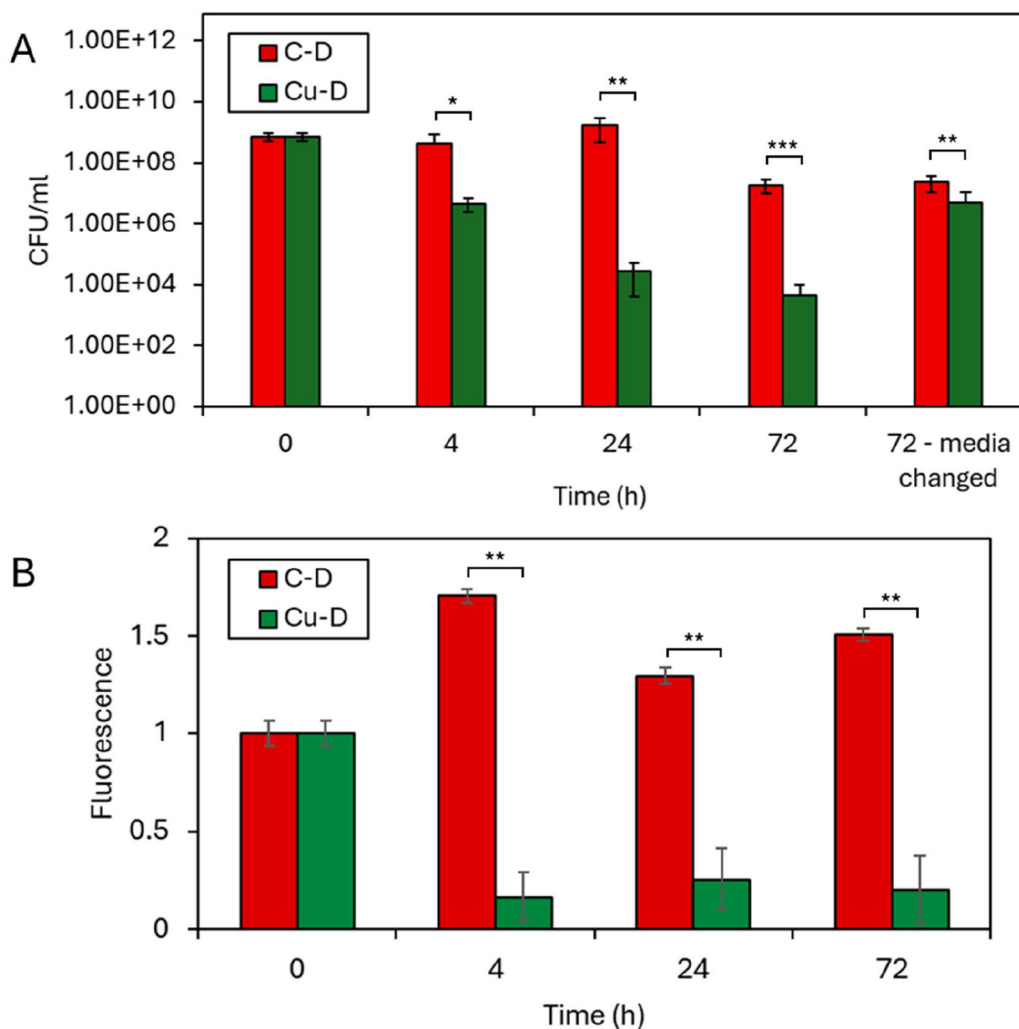


**Figure 5.** Antibacterial properties against *S. aureus* (ATCC6538) measured through (A) CFU count by serial dilution technique and (B) fluorescence (normalized by initial value) revealed by the Presto Blue analysis, for C-D and Cu-D groups. \* p-value < 0.05; \*\* p-value < 0.01; \*\*\* p-value < 0.001.

### 3.9. SEM Imaging

*S. aureus* colonization on C-D and Cu-D surfaces throughout different time intervals (4h, 24h, and 72h) was observed with SEM imaging (Figure 6). At 4h, both C-D and Cu-D samples exhibited a growing bacterial population at the different locations of the samples. After 24h and 72h, bacterial growth in C-D samples could be observed, with an increased population distributed in clusters, compared to the 4h time point where bacteria were sparsely distributed. At each time point, there was no change in the morphology of *S. aureus* for this group. On the Cu-D samples, some bacteria were also observed on the surface for all time points, but no clustering of bacteria was observed at 24h and after. At 24h, the fragmented cytoskeletons of the bacteria suggested the appearance of bacterial damage or stress. After 72 hours, the bacteria on the Cu-D samples were scarcer and more irregularly shaped. The observed changes in bacterial morphology can be attributed to the presence of Cu on the surface, which damages the bacterial membranes. These observations agreed with the outcomes from the CFU counting and Presto Blue analysis, where antibacterial efficacy was demonstrated.

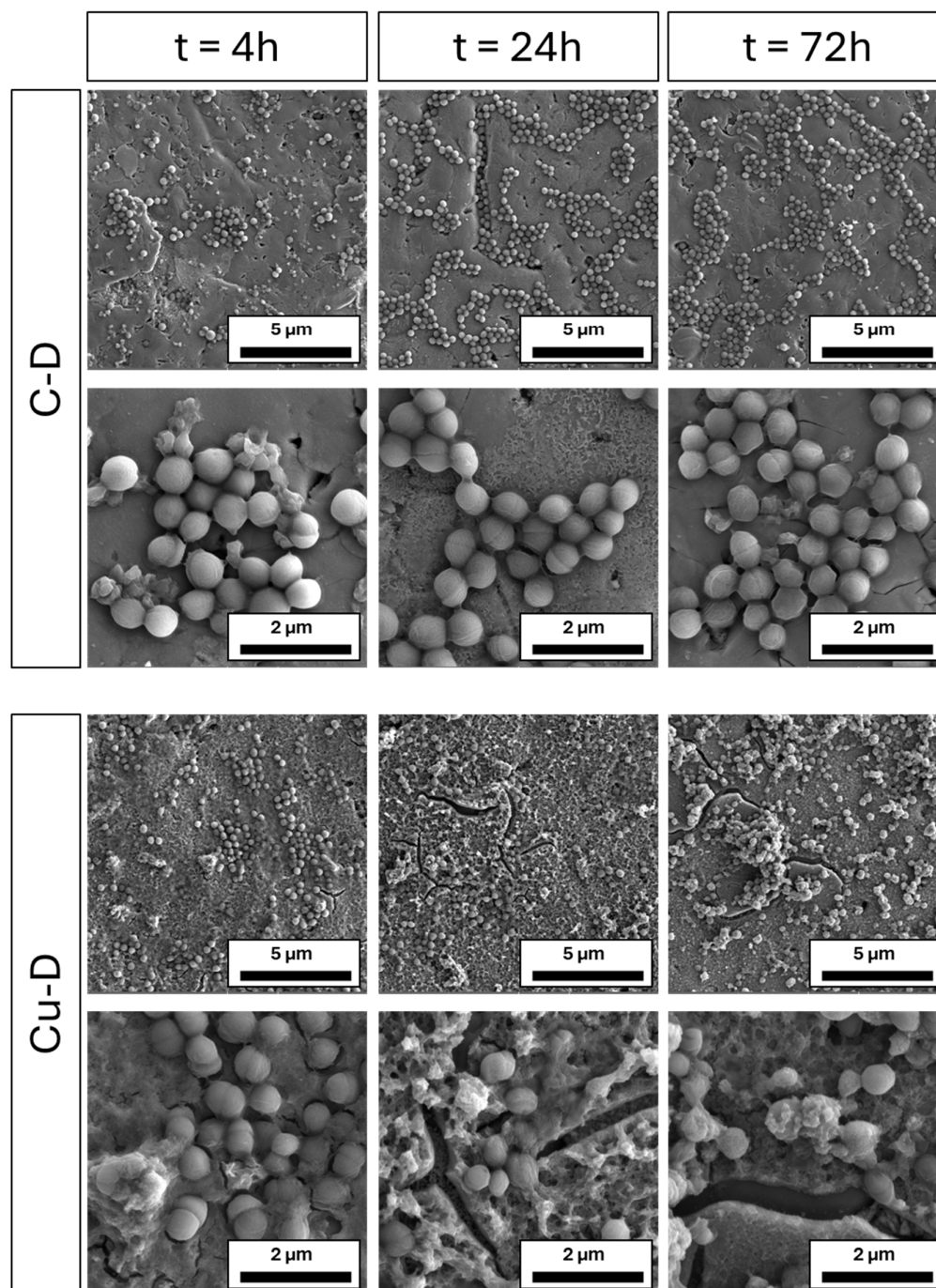


**Figure 6.** Representative SEM images at various time intervals, at 20,000 and 50,000 magnifications, demonstrating the alterations in the morphology of *S. aureus* on Cu-D samples.

### 3.10. Live / Dead Imaging

At each time point, C-D and Cu-D surfaces were stained with Syto9 and PI to differentiate viable and dead bacteria, respectively, and then imaged using a confocal microscope (Figure 7). In the C-D samples group, Syto 9 staining in images taken at 4 hours revealed the presence of viable bacteria, and those taken at 24h showed a growing population. At 24 hours and 72 hours, a vibrant green light was observed, attributed to bacterial growth and a higher cell density. The absence of red colour indicated that no evidence of bacterial death was detected with PI staining in this group. The Cu-D samples exhibited a similar concentration of viable bacteria after 4 hours, along with a minimal presence of dead bacteria. At 24 hours, a rise in the number of dead bacteria and a decrease in the

number of live bacteria were observed. At 72 hours, the trend was similar, with an increase in the presence of vibrant red fluorescence regions. These observations demonstrated that the Cu-D group exhibited antibacterial properties in comparison to the C-D group. The live/dead results combined with the SEM observations from the previous section indicated that the bacteria were able to adhere to the surface despite its hydrophobicity, and that the number of killed bacteria was rising. These observations confirmed the previous analyses obtained in the CFU count, Presto Blue, and SEM analysis.

In summary, compared to a similar study recently published [59], this work extended the surface characterization to elemental analysis with XPS and SEM-EDS, and the bactericidal evaluation by testing a higher bacterial concentration and incorporating an additional timepoint. Elemental analysis confirmed the presence of Cu on the Cu-D surface and provided quantitative measurements. Investigations on the surface roughness and contact angle revealed important properties that could affect bacterial adhesion and proliferation, with Cu-D samples exhibiting enhanced hydrophobicity. The release profile of Cu ions from Cu-D samples evidenced a burst release in the first days, and a progressive decrease up to 14 days. This release profile indicates that the efficiency of the coating probably decreases after three days, which makes biomedical devices using this technology efficient in preventing SSIs infections by reducing the bacteria population in the days that follow the surgery. Additionally, the antibacterial properties of Cu-D surfaces were evaluated *in vitro* against a high dose of *S. aureus*. The results of antibacterial activity with *S. aureus* showed significant 4.8 and 3.6 log<sub>10</sub> reductions at 24 hours and 72 hours. Significant bacterial colonization reductions were also observed in the Presto Blue assay, and two imaging techniques (SEM and live-dead imaging with confocal) showed the presence of dead bacteria with damaged outer membranes.

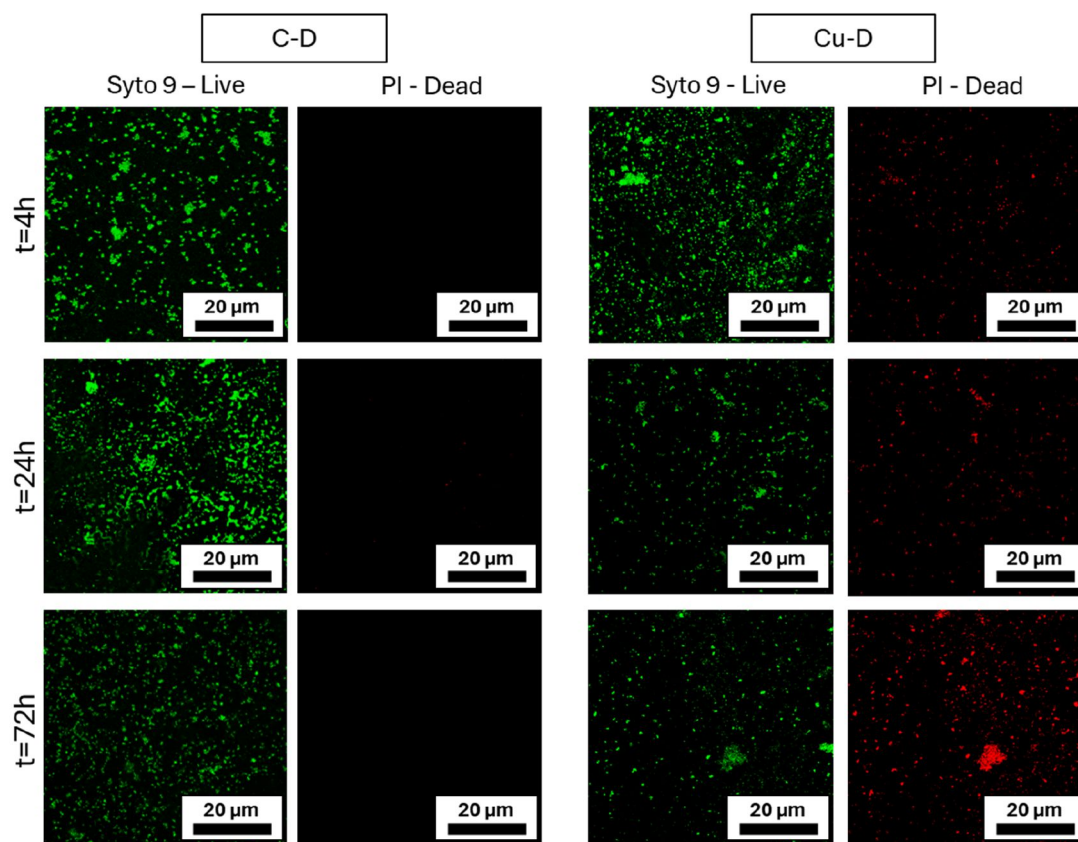


**Figure 7.** Live-dead confocal microscopy images captured at different time points, revealing the distribution of live and dead *S. aureus* on C-D and Cu-D samples.

## 4. Conclusions

The integration of Cu into TiO<sub>2</sub> coatings on titanium substrates represents a paradigm shift in biomedical surface engineering, particularly in the ongoing battle against implant-associated infections. The *in vitro* antimicrobial efficacy of such TiO<sub>2</sub>-Cu coated titanium surfaces is not merely a functional enhancement; it is a biomaterial innovation that aligns biocompatibility with potent, localized antimicrobial activity.

This study characterised the physicochemical properties of a new bactericidal surface consisting of a TiO<sub>2</sub>-Cu coating deposited on Ti alloy by a novel technology. The study also evaluated the antibacterial properties of the Cu-coated surface through a series of assays. Overall, these results demonstrated the *in vitro* bactericidal properties of the technology and justified the need for further development in animal model studies.

In addition to future *in vivo* investigation, which will be a critical step in assessing the antibacterial effect of the coating in a biologically relevant environment and evaluating its potential for clinical applications, further *in vitro* investigations could expand the scope of this study. A Cu coating exhibiting the same hydrophilicity as the control group could reveal the role of the hydrophilicity on the bactericidal efficacy. A limitation of the study is the duration of the bacterial reduction analysis. Here, the assays were conducted up to 72h, but a further evaluation, with timepoints up to one week, could determine if re-population of *S. aureus* on the surface, possibly free of Cu, is possible. If no regrowth is observed, this would indicate potent and long-lasting antibacterial effects. Finally, practical and fundamental questions have arisen during this work. They will inspire future studies on this type of coating, such as the efficacy against other bacterial strains, or if the release kinetics or the bactericidal efficacy are affected by the volume of Cu deposited on the surface.

The TiO<sub>2</sub>-Cu coated titanium surface stands at the convergence of material science, microbiology, and clinical innovation. The development of Cu coatings with intrinsic antibacterial properties for biomedical implant applications has the potential to impact the healthcare system and society at large. As *in vitro* results continue to affirm its efficacy, the challenge now lies in refining its interface with host biology and manufacturing ecosystems. Upon application of this technology to Ti biomedical implants, commercialization of the product, and successful translation into clinical practices, the management of infections in orthopaedic surgery and regenerative medicine could be significantly improved. Future developments could pave the way towards bactericidal implants and improved healthcare delivery. It must be ensured that the leap from bench to bedside is not only scientifically sound but surgically transformative.

**Conflicts of Interest:** SG is employed by Stryker Trauma GmbH. PK received consulting fees from Stryker. All other authors declare that the research underlying this study was carried out without any commercial or financial relationships that could be perceived as a potential conflict of interest.

**Author Contributions:** Conceptualization: MP, SC, SG and DWH; Literature search: MP and SC. Methodology: MP, SC and SG. Investigation and formal analysis: MP and SC. Interpretation of results: MP and SC. Draft preparation: MP and SC. Editing and reviewing: SG, SCC, PK and DWH. Supervision: DWH.

**Acknowledgments:** DWH: MP and SC acknowledge the Australian Research Council for funding of an ARC Industrial Transformation Training Centre in Cell and Tissue Engineering Technologies. SG would like to thank DOT GmbH, especially Dr. Francia Molina and Janine Petters, for surface preparation and coating of the specimens, as well as Dr. Jörg Eschweiler for his critical, iterative review of the manuscript MP and SC would also like to acknowledge the support provided by the Central Analytical Research Facility (CARF) at Queensland University of Technology (QUT), especially the assistance of Dr. Jayanti Mendhi.

**Funding:** Financial support was provided by the Cell and Tissue Engineering Technology - Australian Research Council Centre (grant number: IC190100026), Queensland Institute of Technology, Brisbane, Australia, and Stryker GmbH (Stryker ID: TR-T2AL-ARTI-2147892).

## Supplemental Data

**Table S1.** Elemental composition of the surface of C-D and Cu-D samples upon analysis with EDS, ICP-OES.  $\emptyset$  indicates that the element was not detected.

	EDS		ICP-OES	
	Element	Atomic concentration (%)	Weight concentration (%)	Concentration (mg/ml)
C-D	O	58.8	35.7	$\emptyset$
	Al	4.8	4.9	0.61
	Si	9.2	9.8	1.51
	Ti	25.7	47.0	9.97
	V	1.3	2.6	0.71
	<b>Cu</b>	$\emptyset$	$\emptyset$	$\emptyset$
	Fe	$\emptyset$	$\emptyset$	0.091
	Ca	$\emptyset$	$\emptyset$	0.0047
	Na	$\emptyset$	$\emptyset$	0.10
	Cu-D	O	51.2	27.4
Al		4.0	3.6	0.50
Si		13.3	12.5	1.70
Ti		19.5	31.2	8.18
V		0.9	1.6	0.73
<b>Cu</b>		<b>10.9</b>	<b>23.1</b>	<b>12.64</b>
Fe		$\emptyset$	$\emptyset$	0.11
Ca		$\emptyset$	$\emptyset$	0.085
Na		$\emptyset$	$\emptyset$	0.16

**Table S2.** Elemental composition of C-D and Cu-D obtained with XPS analysis.  $\emptyset$  indicates that the element was not detected.

Elements	O 1s	C 1s	Na 1s	Ti 2p	Si 2p	Cu 2p	Al 2p	
<b>Atomic conc. (%)</b>	<i>C-D</i>	50.5±0.5	22.5±0.2	1.5±0.1	5.5±0.2	19.9±0.3	$\emptyset$	$\emptyset$
	<i>Cu-D</i>	32.9±0.5	31.5±1.5	1.0±0.1	1.5±0.1	12.5±0.2	1.1±0.2	1.9±1.1

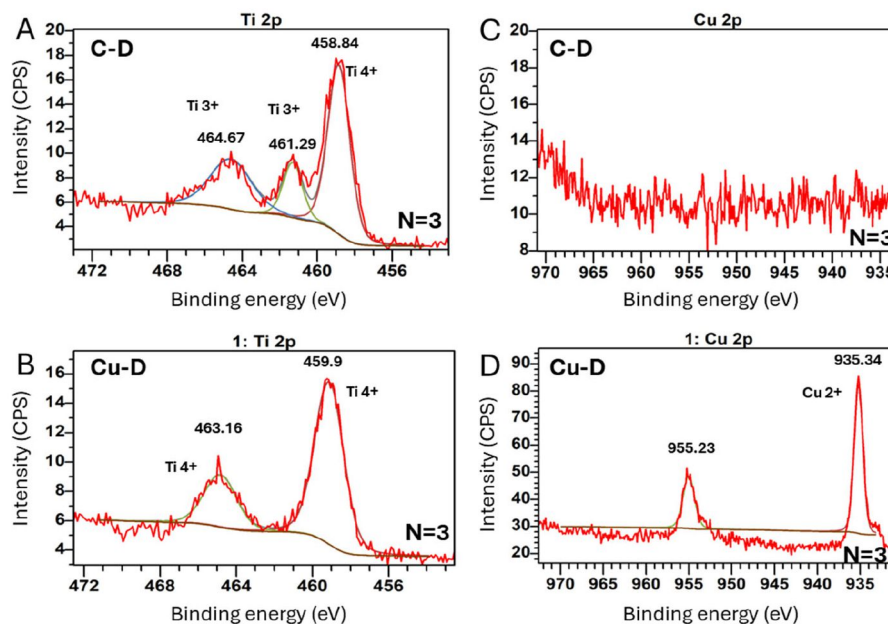


**Figure S1.** Detailed XPS results including: (A) High resolution spectrum of Ti 2p for C-D group, (B) High resolution spectrum of Cu 2p for C-D group, (C) High resolution spectrum of Ti 2p for Cu-D group, (D) High resolution spectrum of Cu 2p for Cu-D group.

## References

1. G. Meroni, A. Tsikopoulos, K. Tsikopoulos, F. Allemanno, P.A. Martino, J.F. Soares Filipe, A journey into animal models of human osteomyelitis: a review, *Microorganisms* 10(6) (2022).
2. T. Miclau, Open fracture management: Critical issues, *OTA International* 3(1) (2020) e074.
3. H. Hoekstra, B. Smeets, W.J. Metsemakers, A.C. Spitz, S. Nijs, Economics of open tibial fractures: the pivotal role of length-of-stay and infection, *Health Econ Rev* 7(1) (2017) 32.
4. I.A. Castillo, J.A. Heiner, R.I. Meremikwu, J. Kellam, S.J. Warner, Where are we in 2022? A summary of 11,000 open tibia fractures over 4 decades, *J Orthop Trauma* 37(8) (2023) e326-e334.
5. J. Li, Q. Wang, Y. Lu, Q. Feng, X. He, M. Li, Zhong, K. Zhang, Relationship between time to surgical debridement and the incidence of infection in patients with open tibial fractures, *Orthopaedic Surgery* 12(2) (2020) 524-532.
6. E.M. Schwarz, J. Parvizi, T. Gehrke, A. Aiyer, A. Battenberg, S.A. Brown, J.J. Callaghan, M. Citak, K. Egol, G.E. Garrigues, M. Ghert, K. Goswami, A. Green, S. Hammond, S.L. Kates, A.C. McLaren, M.A. Mont, S. Namdari, W.T. Obremskey, R. O'Toole, S. Raikin, C. Restrepo, B. Ricciardi, K. Saeed, J. Sanchez-Sotelo, N. Shohat, T. Tan, C.P. Thirukumaran, B. Winters, 2018 International Consensus Meeting on Musculoskeletal Infection: Research Priorities from the General Assembly Questions, *Journal of Orthopaedic Research* 37(5) (2019) 997-1006.
7. A. Bachoura, T.G. Guitton, R.M. Smith, M.S. Vrahas, D. Zurakowski, D. Ring, Infirmity and injury complexity are risk factors for surgical-site infection after operative fracture care, *Clin Orthop Relat Res* 469(9) (2011) 2621-30.
8. A. Trampuz, W. Zimmerli, Diagnosis and treatment of infections associated with fracture-fixation devices, *Injury* 37 Suppl 2 (2006) S59-66.
9. K.V. Dicks, S.S. Lewis, M.J. Durkin, A.W. Baker, R.W. Moehring, L.F. Chen, D.J. Sexton, D.J. Anderson, Surveying the surveillance: surgical site infections excluded by the January 2013 updated surveillance definitions, *Infect Control Hosp Epidemiol* 35(5) (2014) 570-3.
10. R.V. Thakore, S.E. Greenberg, H. Shi, A.M. Foxx, E.L. Francois, M.A. Prablek, S.K. Nwosu, K.R. Archer, J.M. Ehrenfeld, W.T. Obremskey, M.K. Sethi, Surgical site infection in orthopedic trauma: A case-control study evaluating risk factors and cost, *J Clin Orthop Trauma* 6(4) (2015) 220-6.

11. S.M. Kurtz, E. Lau, H. Watson, J.K. Schmier, J. Parvizi, Economic burden of periprosthetic joint infection in the United States, *J Arthroplasty* 27(8 Suppl) (2012) 61-5.e1.
12. W.J. Metsemakers, K. Handojo, P. Reynders, A. Sermon, P. Vanderschot, S. Nijs, Individual risk factors for deep infection and compromised fracture healing after intramedullary nailing of tibial shaft fractures: a single centre experience of 480 patients, *Injury* 46(4) (2015) 740-5.
13. T. Galvain, A. Chitnis, K. Paparouni, C. Tong, C.E. Holy, P.V. Giannoudis, The economic burden of infections following intramedullary nailing for a tibial shaft fracture in England, *BMJ Open* 10(8) (2020) e035404.
14. J.A. Jernigan, Is the burden of *Staphylococcus aureus* among patients with surgical-site infections growing?, *Infect Control Hosp Epidemiol* 25(6) (2004) 457-60.
15. D.J. Anderson, D.J. Sexton, Z.A. Kanafani, G. Auten, K.S. Kaye, Severe surgical site infection in community hospitals: epidemiology, key procedures, and the changing prevalence of methicillin-resistant *Staphylococcus aureus*, *Infect Control Hosp Epidemiol* 28(9) (2007) 1047-53.
16. S.J. McConoughey, R. Howlin, J.F. Granger, M.M. Manring, J.H. Calhoun, M. Shirtliff, S. Kathju, P. Stoodley, Biofilms in periprosthetic orthopedic infections, *Future Microbiol* 9(8) (2014) 987-1007.
17. C.R. Arciola, D. Campoccia, G.D. Ehrlich, L. Montanaro, Biofilm-based implant infections in orthopaedics, *Adv Exp Med Biol* 830 (2015) 29-46.
18. W. Zimmerli, P. Sendi, Orthopaedic biofilm infections, *Apmis* 125(4) (2017) 353-364.
19. C. Llor, L. Bjerrum, Antimicrobial resistance: risk associated with antibiotic overuse and initiatives to reduce the problem, *Ther Adv Drug Saf* 5(6) (2014) 229-41.
20. M.J. Raschke, S.B. Rosslenbroich, T.F. Fuchs, Antibiotic coated nails, in: P.M. Rommens, M.H. Hessmann (Eds.), *Intramedullary nailing: a comprehensive guide*, Springer London, London, 2015, pp. 555-563.
21. S.B. Goodman, Z. Yao, M. Keeney, F. Yang, The future of biologic coatings for orthopaedic implants, *Biomaterials* 34(13) (2013) 3174-83.
22. S. Bohara, J. Suthakorn, Surface coating of orthopedic implant to enhance the osseointegration and reduction of bacterial colonization: a review, *Biomaterials Research* 26(1) (2022) 26.
23. W. Boot, A.L. Foster, O. Guillaume, D. Eglin, T. Schmid, M. D'Este, S. Zeiter, R.G. Richards, T.F. Moriarty, An Antibiotic-Loaded Hydrogel Demonstrates Efficacy as Prophylaxis and Treatment in a Large Animal Model of Orthopaedic Device-Related Infection, *Front Cell Infect Microbiol* 12 (2022) 826392.
24. A.L. Foster, W. Boot, V. Stenger, M. D'Este, A. Jaiprakash, D. Eglin, S. Zeiter, R.G. Richards, T.F. Moriarty, Single-stage revision of MRSA orthopedic device-related infection in sheep with an antibiotic-loaded hydrogel, *Journal of orthopaedic research : official publication of the Orthopaedic Research Society* 39(2) (2021) 438-448.
25. S. Stewart, S. Barr, J. Engiles, N.J. Hickok, I.M. Shapiro, D.W. Richardson, J. Parvizi, T.P. Schaer, Vancomycin-modified implant surface inhibits biofilm formation and supports bone-healing in an infected osteotomy model in sheep: a proof-of-concept study, *J Bone Joint Surg Am* 94(15) (2012) 1406-15.
26. M. Gimeno, P. Pinczowski, G. Mendoza, J. Asín, F.J. Vázquez, E. Vispe, F. García-Álvarez, M. Pérez, J. Santamaría, M. Arruebo, L. Luján, Antibiotic-eluting orthopedic device to prevent early implant associated infections: Efficacy, biocompatibility and biodistribution studies in an ovine model, *Journal of biomedical materials research. Part B, Applied biomaterials* 106(5) (2018) 1976-1986.
27. A. Jorge-Mora, S. Amhaz-Escanlar, S. Fernandez-Pose, A. García-Iglesias, F. Mandia-Mancebo, E. Franco-Trepas, M. Guillán-Fresco, J. Pino-Mínguez, Commercially available antibiotic-laden PMMA-covered locking nails for the treatment of fracture-related infections - A retrospective case analysis of 10 cases, *J Bone Jt Infect* 4(4) (2019) 155-162.
28. D. Inoue, T. Kabata, K. Ohtani, Y. Kajino, T. Shirai, H. Tsuchiya, Inhibition of biofilm formation on iodine-supported titanium implants, *Int Orthop* 41(6) (2017) 1093-1099.
29. Y.Y. Huang, H. Choi, Y. Kushida, B. Bhayana, Y. Wang, M.R. Hamblin, Broad-spectrum antimicrobial effects of photocatalysis using titanium dioxide nanoparticles are strongly potentiated by addition of potassium iodide, *Antimicrob Agents Chemother* 60(9) (2016) 5445-53.

30. E.H. Bosch, H. van Doorne, S. de Vries, The lactoperoxidase system: the influence of iodide and the chemical and antimicrobial stability over the period of about 18 months, *J Appl Microbiol* 89(2) (2000) 215-24.
31. Z. Zhao, Nanosurface modification of Ti64 implant by anodic fluorine-doped alumina/titania for orthopedic application, *Materials Chemistry and Physics* 281 (2022) 125867.
32. S. Yamaguchi, P.T.M. Le, S.A. Shintani, H. Takadama, M. Ito, S. Ferraris, S. Spriano, Iodine-loaded calcium titanate for bone repair with sustainable antibacterial activity prepared by solution and heat treatment, *Nanomaterials* 11(9) (2021) 2199.
33. D. Inoue, T. Kabata, Y. Kajino, T. Shirai, H. Tsuchiya, Iodine-supported titanium implants have good antimicrobial attachment effects, *J Orthop Sci* 24(3) (2019) 548-551.
34. G. Daeschlein, Antimicrobial and antiseptic strategies in wound management, *Int Wound J* 10 Suppl 1(Suppl 1) (2013) 9-14.
35. M. Lollobrigida, S. Filardo, R. Sessa, M. Di Pietro, G. Bozzuto, A. Molinari, L. Lamazza, I. Voza, A. De Biase, Antibacterial activity and impact of different antiseptics on biofilm-contaminated implant surfaces, *Applied Sciences* 9(24) (2019) 5467.
36. A. Tripathy, P. Sen, B. Su, W.H. Briscoe, Natural and bioinspired nanostructured bactericidal surfaces, *Advances in Colloid and Interface Science* 248 (2017) 85-104.
37. S.V. Oopath, A. Baji, M. Abtahi, T.Q. Luu, K. Vasilev, V.K. Truong, Nature-inspired biomimetic surfaces for controlling bacterial attachment and biofilm development, *Advanced Materials Interfaces* 10(4) (2023) 2201425.
38. C.M. Beddoes, C.P. Case, W.H. Briscoe, Understanding nanoparticle cellular entry: A physicochemical perspective, *Advances in Colloid and Interface Science* 218 (2015) 48-68.
39. L. Wang, X. Guo, H. Zhang, Y. Liu, Y. Wang, K. Liu, H. Liang, W. Ming, Recent advances in superhydrophobic and antibacterial coatings for biomedical materials, *Coatings* 12(10) (2022) 1469.
40. D.P. Linklater, E.P. Ivanova, Nanostructured antibacterial surfaces – What can be achieved?, *Nano Today* 43 (2022) 101404.
41. J.A. Lemire, J.J. Harrison, R.J. Turner, Antimicrobial activity of metals: mechanisms, molecular targets and applications, *Nat Rev Microbiol* 11(6) (2013) 371-84.
42. R.J. Turner, Metal-based antimicrobial strategies, *Microb Biotechnol* 10(5) (2017) 1062-1065.
43. M. Birkett, L. Dover, C. Cherian Lukose, A. Wasy Zia, M.M. Tambuwala, Á. Serrano-Aroca, Recent advances in metal-based antimicrobial coatings for high-touch surfaces, *Int J Mol Sci* 23(3) (2022).
44. E. Zhang, X. Zhao, J. Hu, R. Wang, S. Fu, G. Qin, Antibacterial metals and alloys for potential biomedical implants, *Bioactive Materials* 6(8) (2021) 2569-2612.
45. W.R. Fordham, S. Redmond, A. Westerland, E.G. Cortes, C. Walker, C. Gallagher, C.J. Medina, F. Waechter, C. Lunk, R.F. Ostrum, G.A. Caputo, J.D. Hettinger, R.R. Krchnavek, Silver as a bactericidal coating for biomedical implants, *Surface and Coatings Technology* 253 (2014) 52-57.
46. C.E. Santo, D. Quaranta, G. Grass, Antimicrobial metallic copper surfaces kill *Staphylococcus haemolyticus* via membrane damage, *Microbiologyopen* 1(1) (2012) 46-52.
47. S.V. Gudkov, D.E. Burmistrov, D.A. Serov, M.B. Rebezov, A.A. Semenova, A.B. Lisitsyn, A mini review of antibacterial properties of ZnO nanoparticles, *Frontiers in Physics* 9 (2021).
48. S.A. Read, S. Obeid, C. Ahlenstiel, G. Ahlenstiel, The role of zinc in antiviral immunity, *Adv Nutr* 10(4) (2019) 696-710.
49. K. Mijnendonckx, N. Leys, J. Mahillon, S. Silver, R. Van Houdt, Antimicrobial silver: uses, toxicity and potential for resistance, *Biometals* 26(4) (2013) 609-21.
50. Q. Liu, A. Li, S. Liu, Q. Fu, Y. Xu, J. Dai, P. Li, S. Xu, Cytotoxicity of biodegradable zinc and its alloys: a systematic review, *Journal of Functional Biomaterials* 14(4) (2023) 206.
51. M. Vincent, P. Hartemann, M. Engels-Deutsch, Antimicrobial applications of copper, *Int J Hyg Environ Health* 219(7 Pt A) (2016) 585-591.
52. M. Vincent, R.E. Duval, P. Hartemann, M. Engels-Deutsch, Contact killing and antimicrobial properties of copper, *Journal of Applied Microbiology* 124(5) (2018) 1032-1046.

53. G. Grass, C. Rensing, M. Solioz, Metallic copper as an antimicrobial surface, *Applied and Environmental Microbiology* 77(5) (2011) 1541-1547.
54. J.P. Butler, Effect of copper-impregnated composite bed linens and patient gowns on healthcare-associated infection rates in six hospitals, *J Hosp Infect* 100(3) (2018) e130-e134.
55. J.O. Noyce, H. Michels, C.W. Keevil, Potential use of copper surfaces to reduce survival of epidemic meticillin-resistant *Staphylococcus aureus* in the healthcare environment, *J Hosp Infect* 63(3) (2006) 289-97.
56. E.A. Bryce, B. Velapatino, H. Akbari Khorami, T. Donnelly-Pierce, T. Wong, R. Dixon, E. Asselin, In vitro evaluation of antimicrobial efficacy and durability of three copper surfaces used in healthcare, *Biointerphases* 15(1) (2020) 011005.
57. M.K. Charles, T.C. Williams, D. Nakhaie, T. Woznow, B. Velapatino, A.C. Lorenzo-Leal, H. Bach, E.A. Bryce, E. Asselin, In vitro assessment of antibacterial and antiviral activity of three copper products after 200 rounds of simulated use, *BioMetals* (2023).
58. D.A. Montero, C. Arellano, M. Pardo, R. Vera, R. Gálvez, M. Cifuentes, M.A. Berasain, M. Gómez, C. Ramírez, R.M. Vidal, Antimicrobial properties of a novel copper-based composite coating with potential for use in healthcare facilities, *Antimicrobial Resistance & Infection Control* 8(1) (2019) 3.
59. P.M. Giraldo-Osorno, A.B. Turner, S.M. Barros, R. Büscher, S. Gutttau, F. Asa'ad, M. Trobos, A. Palmquist, Anodized Ti6Al4V-ELI, electroplated with copper is bactericidal against *Staphylococcus aureus* and enhances macrophage phagocytosis, *J Mater Sci Mater Med* 36(1) (2025) 14.
60. F. Heidenau, W. Mittelmeier, R. Detsch, M. Haenle, F. Stenzel, G. Ziegler, H. Gollwitzer, A novel antibacterial titania coating: Metal ion toxicity and in vitro surface colonization, *Journal of Materials Science: Materials in Medicine* 16(10) (2005) 883-888.
61. M. Haenle, A. Fritsche, C. Zietz, R. Bader, F. Heidenau, W. Mittelmeier, H. Gollwitzer, An extended spectrum bactericidal titanium dioxide (TiO<sub>2</sub>) coating for metallic implants: in vitro effectiveness against MRSA and mechanical properties, *J Mater Sci Mater Med* 22(2) (2011) 381-7.
62. C. Gargioni, M. Borzenkov, L. D'Alfonso, P. Sperandeo, A. Polissi, L. Cucca, G. Dacarro, P. Grisoli, P. Pallavicini, A. D'Agostino, A. Taglietti, Self-assembled monolayers of copper sulfide nanoparticles on glass as antibacterial coatings, *Nanomaterials* 10(2) (2020) 352.
63. J. Fiedler, A. Kolitsch, B. Kleffner, D. Henke, S. Stenger, R.E. Brenner, Copper and silver ion implantation of aluminium oxide-blasted titanium surfaces: proliferative response of osteoblasts and antibacterial effects, *Int J Artif Organs* 34(9) (2011) 882-8.
64. N.N. Cherenda, A.V. Basalai, V.I. Shymanski, V.V. Uglov, V.M. Astashynski, A.M. Kuzmitski, A.P. Laskovnev, G.E. Remnev, Modification of Ti-6Al-4V alloy element and phase composition by compression plasma flows impact, *Surface and Coatings Technology* 355 (2018) 148-154.
65. G. Zegan, N. Cimpoesu, M. Agop, I. Stirbu, D. Chicet, B. Istrate, A. Alexandru, B. Prisacariu, Improving the HA deposition process on ti-based advanced alloy through sandblasting, *OPTOELECTRONICS AND ADVANCED MATERIALS-RAPID COMMUNICATIONS* 10 (2016) 279-284.
66. A. Yuda, S. Supriadi, A. Saragih, Surface modification of Ti-alloy based bone implant by sandblasting, 2019.
67. A. Polishetty, V. Manoharan, G. Littlefair, C. Sonavane, Machinability assessment of Ti-6Al-4V for aerospace applications, *ASME Early Career Technical Journal* 12 (2013) 53-58.
68. T. Liang, Y. Wang, L. Zeng, Y. Liu, L. Qiao, S. Zhang, R. Zhao, G. Li, R. Zhang, J. Xiang, F. Xiong, A. Shanaghi, H. Pan, Y. Zhao, Copper-doped 3D porous coating developed on Ti-6Al-4V alloys and its in vitro long-term antibacterial ability, *Applied Surface Science* 509 (2020) 144717.
69. X. Zhou, G.E. Thompson, P. Skeldon, K. Shimizu, H. Habazaki, G.C. Wood, The valence state of copper in anodic films formed on Al-1at.% Cu alloy, *Corrosion* 47 (2005) 1299-1306.
70. S.S.d. Rocha, G.L. Adabo, G.E.P. Henriques, M.A.d.A. Nóbilo, Vickers hardness of cast commercially pure titanium and Ti-6Al-4V alloy submitted to heat treatments, *Brazilian Dental Journal* 17 (2006).
71. Mulyadi, R. Ramlan, S. Aini, Djuhana, Effect of various sintering temperature of ceramic TiO<sub>2</sub> on physical properties and crystall structure, *Journal of Physics: Conference Series* 1282 (2019) 012049.
72. Y. Jianchao, G. Wang, Y. Rong, Experimental study on the surface integrity and chip formation in the micro cutting process, *Procedia Manufacturing* 1 (2015) 655-662.

73. C.J. Chen, S.J. Ding, C.C. Chen, Effects of surface conditions of titanium dental implants on bacterial adhesion, *Photomed Laser Surg* 34(9) (2016) 379-88.
74. J.P. Ruparelia, A.K. Chatterjee, S.P. Duttagupta, S. Mukherji, Strain specificity in antimicrobial activity of silver and copper nanoparticles, *Acta Biomaterialia* 4(3) (2008) 707-716.

**Disclaimer/Publisher's Note:** The statements, opinions and data contained in all publications are solely those of the individual author(s) and contributor(s) and not of MDPI and/or the editor(s). MDPI and/or the editor(s) disclaim responsibility for any injury to people or property resulting from any ideas, methods, instructions or products referred to in the content.